NeuroImage: Clinical 22 (2019) 101713

Contents lists available at ScienceDirect

NeuroImage: Clinical

journal homepage: www.elsevier.com/locate/ynicl

Hypercapnic BOLD MRI compared to $H_2{}^{15}O$ PET/CT for the hemodynamic evaluation of patients with Moyamoya Disease

Till-Karsten Hauser[a], Achim Seeger[a], Benjamin Bender[a], Uwe Klose[a], Johannes Thurow[c], Ulrike Ernemann[a], Marcos Tatagiba[b], Philipp T. Meyer[c], Nadia Khan[b,d,*], Constantin Roder[b]

[a] Department of Neuroradiology, Eberhard Karls University Tübingen, Germany
[b] Department of Neurosurgery, Eberhard Karls University Tübingen, Germany
[c] Department of Nuclear Medicine, Medical Center – University of Freiburg, Faculty of Medicine, University of Freiburg, Freiburg, Germany
[d] Moyamoya Center, Division of Pediatric Neurosurgery, University Children's Hospital Zürich, Switzerland

ARTICLE INFO

Keywords:
Moyamoya
PET/CT
Cerebrovascular reserve
BOLD MRI

ABSTRACT

Background and purpose: Patients with Moyamoya Disease (MMD) need hemodynamic evaluation of vascular territories at risk of stroke. Today's investigative standards include $H_2{}^{15}O$ PET/CT with pharmacological challenges with acetazolamide (ACZ). Recent developments suggest that CO_2-triggered blood-oxygen-level-dependent (BOLD) functional MRI might provide comparable results to current standard methods for evaluation of territorial hemodynamics, while being a more widely available and easily implementable method. This study examines results of a newly developed quantifiable analysis algorithm for CO_2-triggered BOLD MRI in Moyamoya patients and correlates the results with $H_2{}^{15}O$ PET/CT with ACZ challenge to assess comparability between both modalities.

Methods: CO_2-triggered BOLD MRI was performed and compared to $H_2{}^{15}O$ PET/CT with ACZ challenge in patients with angiographically proven MMD. Images of both modalities were analyzed retrospectively in a blinded, standardized fashion by visual inspection, as well as with a semi-quantitative analysis using stimuli-induced approximated regional perfusion-weighted data and BOLD-signal changes with reference to cerebellum.

Results: 20 consecutive patients fulfilled the inclusion criteria, a total of 160 vascular territories were analyzed retrospectively. Visual analysis (4-step visual rating system) of standardized, color-coded cerebrovascular reserve/reactivity maps showed a very strong correlation (Spearman's rho = 0.9, $P < 0.001$) between both modalities. Likewise, comparison of approximated regional perfusion changes across vascular territories (normalized to cerebellar change) reveal a highly significant correlation between both methods (Pearson's $r = 0.71$, $P < 0.001$).

Conclusions: The present analysis indicates that CO_2-triggered BOLD MRI is a very promising tool for the hemodynamic evaluation of MMD patients with results comparable to those seen in $H_2{}^{15}O$ PET/CT with ACZ challenge. It therefore holds future potential in becoming a routine examination in the pre- and postoperative evaluation of MMD patients after further prospective evaluation.

1. Introduction

Moyamoya Disease (MMD) is characterized by a bilateral progressive stenosis of the Circle of Willis with fine collateral networks resembling a puff of smoke, giving the disease its name (Suzuki and Takaku, 1969). The most common initial symptoms are transient ischemic attacks (TIAs) and ischemic or hemorrhagic strokes caused by an insufficient cerebral perfusion. To prevent recurrence of such events, microsurgical revascularization is indicated in many patients (Khan et al., 2003; Scott and Smith, 2009; Guzman et al., 2009). Before indicating a surgical revascularization, identification of cerebral vascular territories with insufficient perfusion is crucial to ensure a successful tailored treatment for each patient. This, however cannot be achieved with routine MRI and digital subtraction angiography (DSA) alone, but hemodynamic modalities like $H_2{}^{15}O$ positron emission tomography (PET) or Single Photon Emission Computed Tomography (SPECT) with acetazolamide (ACZ) challenge, among others, remain indispensible (Pandey and Steinberg, 2011; Lee et al., 2009; Roder et al., 2018; Acker

* Corresponding author at: Center for Moyamoya and Cerebral Revascularization Tübingen & Moyamoya Center, University Children's Hospital Zurich, Hoppe-Seyler-Str. 3, 72076 Tübingen, Germany.
E-mail address: moyamoya@neurochirurgie-tuebingen.de (N. Khan).

https://doi.org/10.1016/j.nicl.2019.101713
Received 18 November 2018; Received in revised form 14 January 2019; Accepted 3 February 2019
Available online 04 February 2019

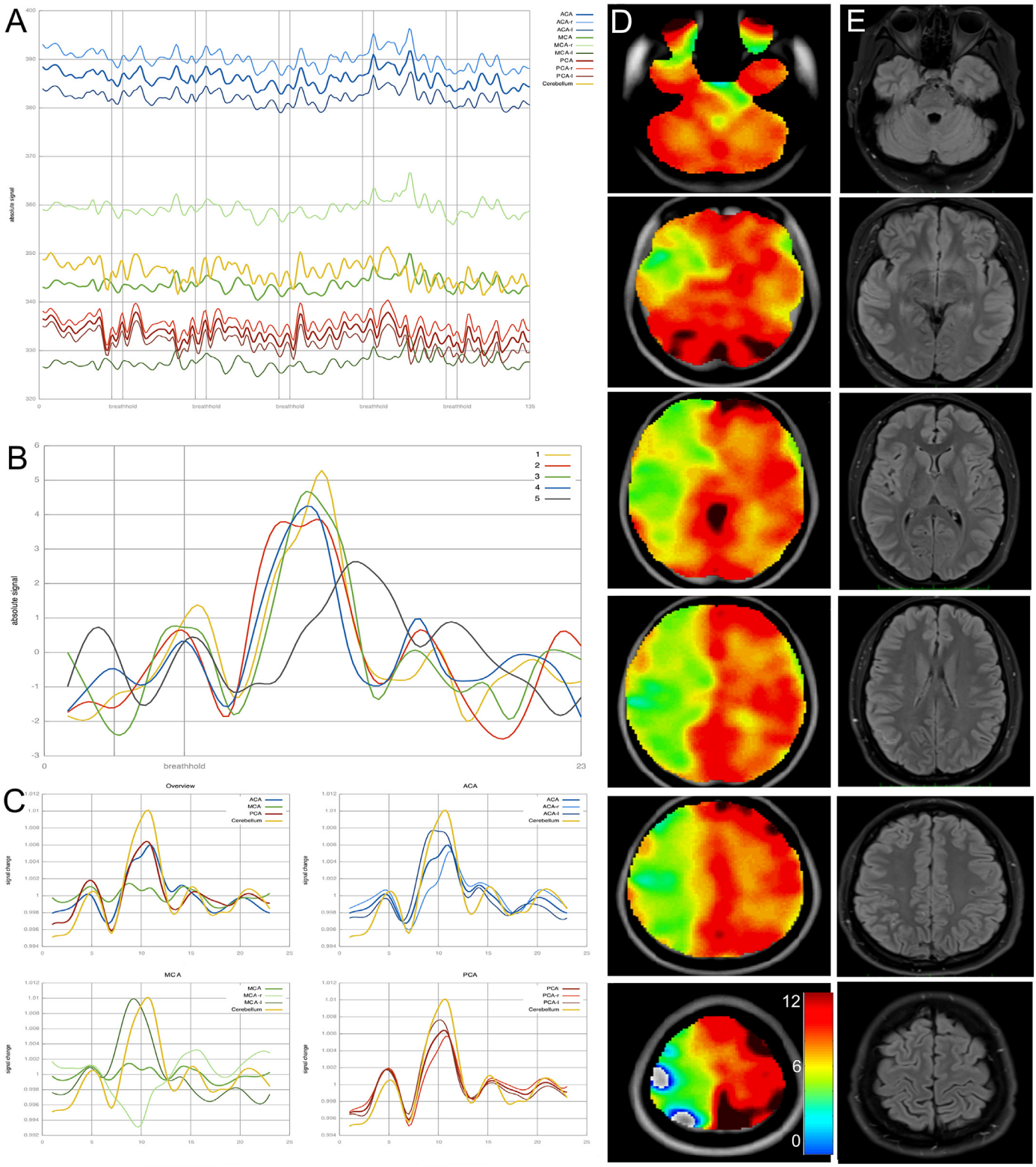

Fig. 1. A) Plot of mean signal intensities in all evaluated regions over the course of the whole fMRI measurement. Vertical lines show the breath-hold time periods of 9 s each. B) Shows response curves of the cerebellum as a reference. In this case, the fifth cycle (grey color) shows a markedly different response curve suggestive of poor patient compliance in this cycle. For further analysis this cycle was excluded. C) Peristimulus histograms (PSTH) showing breath hold related signal increase in the ACA (blue), MCA (green) and PCA (red) territories compared to the reference curve of the cerebellum (yellow). Top left shows an overview with mean curves representing the ACA, MCA and PCA signals of both hemispheres. This patient with unilateral involvement of Moyamoya angiopathy shows nearly normal response curves in the left MCA, whereas there is a negative curve amplitude in the right sided MCA territory, indicating flow reduction during breath hold- induced vessel dilatation. D) CVR maps of breath-hold BOLD MRI indicating the above-mentioned vascular deficits. Values for the color-scale resemble the integral of the relative signal change of BOLD MRI. E) Corresponding FLAIR images. (For interpretation of the references to color in this figure legend, the reader is referred to the web version of this article.)

et al., 2018). Main disadvantages of $H_2{}^{15}O$ PET with ACZ challenge include high costs and limited availability. Although the radiation exposure due to injection of $H_2{}^{15}O$ is very low (especially with modern scanners) and side-effects due to ACZ are very rare and usually transient, this may be of concern in special patients (e.g., in pediatric patients). Throughout the last decades new approaches have been pursued to overcome some of these drawbacks. More advanced imaging attempts used MR-based arterial spin labeling (ASL), CO_2-triggered blood-oxygen-level-dependent (BOLD) and even resting-state functional MRI techniques, which could be used without any intravenous contrast agent injections (Liu et al., 2017; Shiino et al., 2003; Sam et al., 2015; Pellaton et al., 2016; Mikulis et al., 2005; Mazerolle et al., 2018; Mandell et al., 2008; Heyn et al., 2010; van Niftrik et al., 2016; Fierstra et al., 2013; Donahue et al., 2014; Bright and Murphy, 2013; Fierstra et al., 2018). A contemporary consensus statement of different imaging methods for diagnosis and evaluation of cerebrovascular disease was recently published by Donahue et al. (2018) Of these, CO_2-triggered BOLD MRI seems to be one of the most promising tools for evaluation of cerebral hemodynamics. This technique uses the physiological vasodilatory effect of CO_2 to alter the amount of deoxy-hemoglobin in venules by blood flow increase due to arteriole smooth-muscle-cell relaxation with constant cerebral metabolic rate of oxygen, which can be measured with BOLD MRI. Therefore, the change between baseline BOLD signal can be compared to the signal after CO_2-triggered vasodilation, resulting in a signal change which is most commonly called the cerebrovascular reactivity (CVR) (Liu et al., 2017; Heyn et al., 2010). Triggers for the changes of CO_2 concentrations can either be exogenous with breathing masks delivering different concentrations of gas, or endogenous by breathing pauses – commonly called breath-hold (Fierstra et al., 2013).

In the present retrospective study, we thus pursued a systematic comparison of the cerebral perfusion reserve (CPR), measured with $H_2{}^{15}O$ PET/CT with ACZ challenge, and CO_2-triggered BOLD MRI for assessment of CVR in patients with MMD. To this end, we compared not only standardized, color-encoded CPR and CVR maps gained by both modalities (as done in clinical routine) but also contemplated the correlation between approximated regional perfusion changes across vascular territories.

2. Material and methods

A retrospective analysis of consecutive adult patients at our Moyamoya Center was performed. Main inclusion criteria were angiographically proven Moyamoya angiopathy, the availability of $H_2{}^{15}O$ PET/CT with ACZ challenge and a CO_2-triggered BOLD MRI with a chronological proximity of both examinations of < 6 months with no surgical intervention in-between. Pre- and postoperative examinations were included, the analysis was performed combined and in subgroups. If indicated, the surgical intervention was performed by a direct STA-MCA and/or direct or indirect STA-ACA (EDAS - encephala-duro-arterio-synangiosis or EGPS – encephalo-galea-periost-synagiosis) bypass. Ethical approval was obtained at the University of Tübingen Ethics Committee. General patient data were obtained from the patients' clinical files, any imaging data was stored and analyzed in the hospital's PACS system.

2.1. MR data acquisition

All MR images were acquired on a 3 T MR Scanner (Magnetom Skyra, Siemens, Erlangen, Germany) using a 20-channel head coil during a routine clinical MRI scan. The dynamic data was measured by means of a whole brain 2D T2*-weighted echo-planar sequence scanned parallel to the anterior-posterior commissure. (TR = 3000 ms, TE = 36 ms, matrix 96 × 96, 3 mm slice thickness, 34 slices in interleaved ascending order, FOV = 245 mm, resolution 2.6 × 2.6 × 3.0, TA 6:53, 135 measurements). The protocol consisted of 60 s of normal breathing (20 measurements) followed by 5 repetitive cycles of 9 s breath-hold in expiration (3 measurements) and 60 s of regular breathing (20 measurements) (see also Fig. 1). The patient breathing instructions were presented visually via a wall-mounted display and a mirror fixed to the head coil. Presentation V20.1 (Neurobehavioral Systems, Berkeley, CA, USA) was used to present scanner triggered stimuli.

2.2. MR data processing

Preprocessing of the resulting 135 functional datasets was performed in SPM12 (The Wellcome Dept. of Imaging Neuroscience, London; www.fil.ion.ucl.ac.uk/spm). After conversion of DICOM images to nifti format, slice timing correction was used to equalize time of image acquisition. Images were then realigned so that patient head movements were compensated. As the last step the datasets were spatially normalized to a standard MNI (Montreal Neuroimaging Institute) space and smoothed by a 12 mm full with half maximum filter.

2.3. MR map and curve calculation

The data was further analyzed by a script programmed in MATLAB R2017b (The MathWorks, Inc., Natick, Massachusetts; http://www.mathworks.com).

The ATT (arterial transit time) (Mutsaerts et al., 2015) based flow territory atlas was used to generate volumes of interest (VOIs) for anterior cerebral artery (ACA left and right), middle cerebral artery (MCA left and right), posterior cerebral artery (PCA left and right) and cerebellar vascular territories (left and right). Raw data of signal change for each territory in relation to the breath-hold cycles is displayed in Fig. 1A.

Mean cerebellar signal intensity of the fMRI data was calculated and displayed for all 5 breath-hold cycles (Fig. 1B). This was used to verify patient compliance and overall signal quality. At this time, individual breath-hold cycles could be excluded from further evaluation if the reference signal (cerebellum) showed no suitable signal curve in visual inspection (Fig. 1B, grey curve).

All included breath-hold cycles were averaged. With the resulting respective 23 fMRI datasets a VOI-mean was calculated, which was then used to set the beginning and end points of the breath-hold related signal increase. As the time of onset of the breath-hold related flow response varied in patients (different physiological characteristics, chronologic variation in collaboration of starting to hold the breath), the reference VOI (cerebellum) was used to manually set the start and end timepoint of the flow response.

For each voxel (volume element) in the 3D dataset, the signal curve was de-trended to remove linear signal changes over time. The relative signal change was then computed by dividing the signal at each point in the curve by the curve mean to account for differences in initial signal intensity of the *epi* imaging sequence. This time-course of signal intensity was then displayed as signal change for each vascular territory (Fig. 1C).

After up-sampling the data, the integral of the curve between the start and end point was calculated for each voxel resulting in a 3D integral map which was then displayed as an overlay on a normalized standard brain (Fig. 1D).

2.4. $H_2{}^{15}O$ PET/CT with ACZ challenge

PET scans were acquired either on a Philips Gemini TF64 PET/CT (n = 14; until 12/2017) or a Philips Vereos digital PET/CT system (n = 6; from 01/2018 onward; Philips, The Netherlands). We did not pursue absolute quantification of regional cerebral blood flow (CBF; in terms of ml/min/100 g brain tissue) by continuous arterial blood sampling and kinetic modeling. Instead we used a simplified method to estimate cerebral perfusion reserve (CPR) as proposed by Arigoni et al.

(2000) After a low-dose CT for attenuation correction, four 4-min scans were acquired per patient. The head position was gently restrained by a tape, carefully monitored and, if necessary, corrected throughout the procedure by means of reference skin marks and the scanner laser beam. Scans before and after ACZ injection were done in duplicate (10-min interval between $H_2{}^{15}O$ injections to allow for sufficient decay) under resting conditions (i.e., eyes open and ears unplugged at normal ambient light and noise). A standard dose of 1000 mg ACZ (except in three patients who received 500 to 800 mg because of low body weights of 44–57 kg) was dissolved in 50 ml water for injection and administered immediately after the end of the 2nd baseline scan as an infusion over 5 min. The 3rd PET scan was started 10 min (5 min) after the start (end) of the ACZ infusion. A standard dose of 300 MBq $H_2{}^{15}O$ (10 ml volume) (except in one patient with low body weight examined with the Vereos scanner, who received 250 MBq per injection) was injected at the start of each PET scan as a bolus over 3 s into a cubital vein. Data sets of the Gemini scanner were reconstructed using the line-of-response row-action maximum likelihood expectation algorithm (LOR-RAMLA) 3D iterative reconstruction algorithm (number of iterations = 3, number of subsets = 33, resulting voxel size = 2.0 × 2.0 × 2.0 mm^3) into a dynamic sequence of 15 frames (6 × 5 s, 3 × 10 s, 3 × 20 s, 2 × 30 s and 1 × 60 s), whereas the data of the Vereos scanner were reconstructed by using line-of-response time-of-flight ordered subsets 3D iterative reconstruction algorithm employing spherically symmetric basis functions (so-called BLOB-OS-TF reconstruction; number of iterations = 3, number of subsets = 11, resulting voxel size = 2.0 × 2.0 × 2.0 mm^3) yielding a dynamic sequence of 30 frames (18 × 5 s, 9 × 10 s and 3 × 20 s) per scan. All datasets were fully corrected (attenuation, scatter, randoms, normalization and calibration) during iterative reconstruction.

For simplified voxel-wise calculation of CPR maps, all scans of each subject were corrected for motion and integrated over 60 s (Vereos) or 70 s (Gemini) after arrival of the tracer in the individual patient's brain (Arigoni et al., 2000). The start time of integration was determined by analyzing the time-activity curve with a whole brain region of interest (ROI; 35% of maximum isodensity contour) covering a 5-cm slab at the level of the basal ganglia. Voxel-wise estimate of CPR (CPR map) were calculated using the SISCOM methodology (O'Brien et al., 1998). In brief, the two integral scans before and after ACZ were averaged and then masked using a threshold of 25% of the image maximum (whole-brain segmentation). Voxel-wise signal change (in percent) from baseline status to the status after ACZ administration was calculated and the resulting parametric map was smoothed (Gaussian filter, 12 mm FWHM) and masked again (see above), yielding the desired CPR map. For visual reads, the average integrated scans before and after ACZ and the CPR map were co-registered to the patients' MRI and displayed in a standardized fashion (typically 32 transaxial planes covering the entire brain; average integrated scans were displayed using an identically thresholded “rainbow” color-scale, while a “cold” color-scale was used for CVR maps). Finally, for ROI analysis of vascular territories, aforementioned images were normalized to the MNI-152 PET template and a ROI set comprising bilateral ACA, MCA and PCA territories (ATT based flow territories, Tatu et al. (1998)) was applied. Since this ROI template lacks ROIs for bilateral striatum, thalamus and cerebellum, these ROIs were generated from the adult brain maximum probability map ‘Hammersmith atlas n30rb83’ (Hammers et al. (2003) for striatum and thalamus) and the SUIT atlas (Diedrichsen (2006) for cerebellum). Accurate ROI alignment was verified by visual inspection in all cases. The commercial software packages PMOD (version 3.7; PMOD Technologies LLC, Switzerland) and Matlab (The MathWorks, Inc., Natick, Massachusetts, United States), as well as the freely available Statistical Parametric Mapping (SPM 12, http://www.fil.ion.ucl.ac.uk/spm/) were used for the aforementioned analyses.

2.5. Comparative analysis of PET and MR BOLD data

A blinded analysis of all CPR and CVR color maps (PET and Breath hold fMRI) was performed independently by two experienced neuroradiologists. Each vascular territory (anterior-(ACA), middle-(MCA), posterior-(PCA) cerebral artery as well as cerebellar) was graded separately for each hemisphere. The visual grading was based on four grades according to each territory's reserve/reactivity: 1) normal 2) mild decrease in cerebrovascular reserve/reactivity 3) strong decrease in cerebrovascular reserve/reactivity 4) no or negative cerebrovascular reserve/reactivity compared to normal.

The interrater-reliability was calculated. Evaluation of any territory with differing results between both raters, was decided in consensus with a third rater.

For the semi-quantitative comparison of perfusion changes, the approximated relative regional perfusion change (percentage change between baseline and ACZ or CO_2 trigger) was assessed by both modalities for each supratentorial vascular territory (separated by site) as well as the cerebellum. Furthermore, approximated relative regional perfusion changes were normalized to the cerebellar perfusion change for optimal comparability of both modalities. This was done to remove systematic individual (e.g., day-to-day variations) and methodological (e.g., different magnitude of vasodilatatory stimulation) variations, which should affect supratentorial target regions and the reference regions to a similar extent and, thus, cancel out.

Additionally, we have separated the analysis in two patient groups, namely pre- and postoperative (after surgical revascularization) examinations. This is based on the fact, that the validity of CO_2 BOLD imaging should be proven for both cohorts separately.

2.6. Statistical analysis

Data was analyzed with Graph Pad Prism (v7.04, GraphPad Software Inc., La Jolla, CA, USA). Categorical data were presented as frequencies, inter-rater agreement was calculated using Cohen's kappa statistics with weighted analysis. Correlation of data was calculated with Pearson's and Spearman's correlation coefficient (r and rho, respectively) for parametric and non-parametric samples, respectively. The two-tailed p-value was accepted to be significant at $p < 0.05$.

3. Results

Twenty consecutive MMD patients fulfilled the inclusion criteria. General clinical data can be found in Table 1. The total number of vascular territories analyzed was 160. If patients had a surgical revascularization, the postoperative imaging took place at least one year after the surgery. CO_2 triggered BOLD MRI was accurately performed in all patients, as supported by the visual analysis of the cerebellar BOLD signal curves. $H_2{}^{15}O$ PET with ACZ challenge showed adequate response of ACZ in all patients (average cerebellar CPR 34 ± 11%).

3.1. Correlation analysis of visual inspection of anatomical color maps

Cohen's Kappa (weighted) for the interrater-agreement between

Table 1
Overview of general patient data.

General patient data	
Mean age (range)	40.2 (16–67)
Female:Male ratio	18:2
Unilateral Moyamoya Angiopathy	5 (25%)
Bilateral Moyamoya Disease	15 (85%)
Imaging before revascularization	11 (55%)
Imaging after revascularization	9 (45%)
Revascularized territories at the time of imaging (range)	22 (1–4)

Table 2
A: Overview of frequency of grade of disease-affection of the respective territories for each modality. B: Over- and underestimation of the respective modalities shown by diverse ratings of individual territories of each modality. The table shows the number of territories with differing estimation of the respective grade (1–4) of the cerebrovascular reserve/reactivity between both modalities. No specific patterns of over- and/or underestimation in each of both modalities could be seen.

A

Grade of affection	*fMRI*	*PET*
1	91	89
2	25	27
3	23	24
4	21	20

B

Over- and underestimation	*fMRI*	*PET*	*Number of territories*
(grade found in respective imaging modality)	1	2	8
	2	1	6
	2	3	3
	3	2	3
	3	4	2
	4	3	3
Total			25

both raters was 0.95, indicating excellent agreement. The visual analysis of signal change in the respective vascular territory on color-coded maps revealed very strong correlation of the results of CO_2 BOLD MRI and $H_2{}^{15}O$ PET/CT with ACZ challenge (rho = 0.90, $p < 0.001$). Differences between the visual ratings (grade 1–4) between both modalities were found in 25 of 160 (15.6%) territories, all these differed by only one grade. The correlation was comparably good for groups separated to pre- (rho = 0.90, $p < 0.001$) and postoperative (rho = 0.91, $p < 0.001$) cohorts. Table 2A shows the distribution of affected vascular territories for both modalities according to the visual analysis. We have also analyzed all territories in which the results of CO_2 BOLD MRI and PET differed. The results can be found in Table 2B. In summary, we did not see a systematic difference in terms of over- or underestimation of any of both technologies in comparison to the other.

3.2. Correlation analysis of approximated regional perfusion changes

The analysis of absolute values of signal change in the respective territories did not show a very high correlation due to the diversity of signal-source in image acquisition by BOLD MRI and PET. There was a weak, albeit significant correlation between approximated regional perfusion/reactivity changes yielded by both modalities across the territories in all patients ($r = 0.35$, $p = 0.001$; Fig. 2A).

3.3. Correlation analysis of approximated regional perfusion/reactivity changes normalized to cerebellum

For semi-quantifiable correlation of BOLD MRI (cererbrovascular reactivity) and PET (cererbral perfusion reserve) data were normalized to the cerebellum. The analysis of all 120 supratentorial vascular territories revealed a strong, highly significant correlation between both imaging modalities ($r = 0.71$, $p < 0.001$). Separate analysis of pre- and postoperative subgroups yielded similar results ($r = 0.61$, $p < 0.001$ and $r = 0.76$, $p < 0.001$, respectively; Fig. 2B–D).

4. Discussion

CO_2-triggered BOLD MRI has developed significantly since its first descriptions and has the potential to become a routine tool for the evaluation of the cerebrovascular reactivity in the future (Liu et al., 2017; Shiino et al., 2003; Sam et al., 2015; Pellaton et al., 2016; Mikulis et al., 2005; Mazerolle et al., 2018; Mandell et al., 2008; Heyn et al., 2010; van Niftrik et al., 2016; Fierstra et al., 2013; Donahue et al., 2014; Bright and Murphy, 2013; Kastrup et al., 2001). The studies performed to date have focused on the image-acquisition techniques and their optimization as well as aim at critically comparing it with other imaging modalities. In MMD where the patients vary in severity of angiopathy and collateral formation, the evaluation of cerebral reserve capacity is not possible with angiography and MRI alone (Roder et al., 2018), hence necessitating additional hemodynamic imaging such as $H_2{}^{15}O$ PET with ACZ challenge. Less expensive, without the need of an intravenous injection, more widely available and easy to implement BOLD MRI may be able to substitute these in the future.

In the present study we demonstrate a highly significant, good to excellent correlation between regional assessments of CPR by H215O PET/CT with ACZ challenge and CVR assessment with breath-hold BOLD MRI in MMD patients based on visual ratings (rho = 0.9; no systematic difference) and normalized regional analyses ($r = 0.71$).

4.1. Selection of stimulus for CO_2-changes in the BOLD-based measurement of cerebrovascular reserve

We used the breath-hold technique to trigger hypercapnia, which results in cerebral vasodilatation and therefore enables the evaluation the CVR. No doubt, this technique, relying on the cooperation of patients and on individual physiological factors (i.e. individual lung size and metabolism) is not a strictly standardized stimulus. Fierstra and colleagues discussed the issue of measuring the CVR with the best stimulus extensively, and conclude that vasoactive substances (such as ACZ), medically induced hypotension and breath-hold triggered hypercapnia are not appropriate for reproducible results, and recommend the use of a computer-controlled gas delivery system for repeatable vasoactive stimuli (Fierstra et al., 2013). Of note, the possible inter-individual variation and the difference between both stimuli (breath-hold and ACZ) also motivated us to contemplate normalized regional CVR estimates.

We agree that a controlled gas delivery system would eliminate the need for patient cooperation thus might lead to more reliable results also in patients with limited compliance. However, patients with such limited compliance might also not be able to remain without relevant head movement for the time of scanning without sedation and might therefore be generally inappropriate for this examination. A recent study proved that also children with a mean age of 12 years were able to collaborate in repeated breath-hold MR examination with good correlation (Dlamini et al., 2018).

Computer-controlled gas delivery devices are not widely available and need patient monitoring during CO_2 administration. Also, the baseline $EtCO_2$ might be manipulated by closed rebreathing systems, which might also bias the results of such examinations. FMRI using breath-hold as a vasodilatory trigger can be performed at nearly every hospital since most (all) modern scanners are able to acquire 2D *epi* images and patient instructions can be presented visually or via spoken instructions through the headphones.

To overcome above-mentioned disadvantages of a gas-delivery system and if the evaluation of the CVR of an individual patient is the goal, the breath-hold technique as used here seems reliable and sufficient. We have control of adequate application of the stimulus / patients' cooperation by analyzing the change of the BOLD signal over 5 breath-hold cycles by visual inspection of the cerebellum data. If individual cycles do not have an adequate signal change for any reason, they can be excluded from the analysis. Further, by analyzing the semi-quantitative cerebellar quotient, absolute inter-individual physiologic changes to a stimulus are less meaningful due to intra-individual results of each examination.

However, if the answer of specific physiologic questions or absolute comparability between individuals are the goal of an examination or study, a replicable and controllable stimulus fitted to each individual

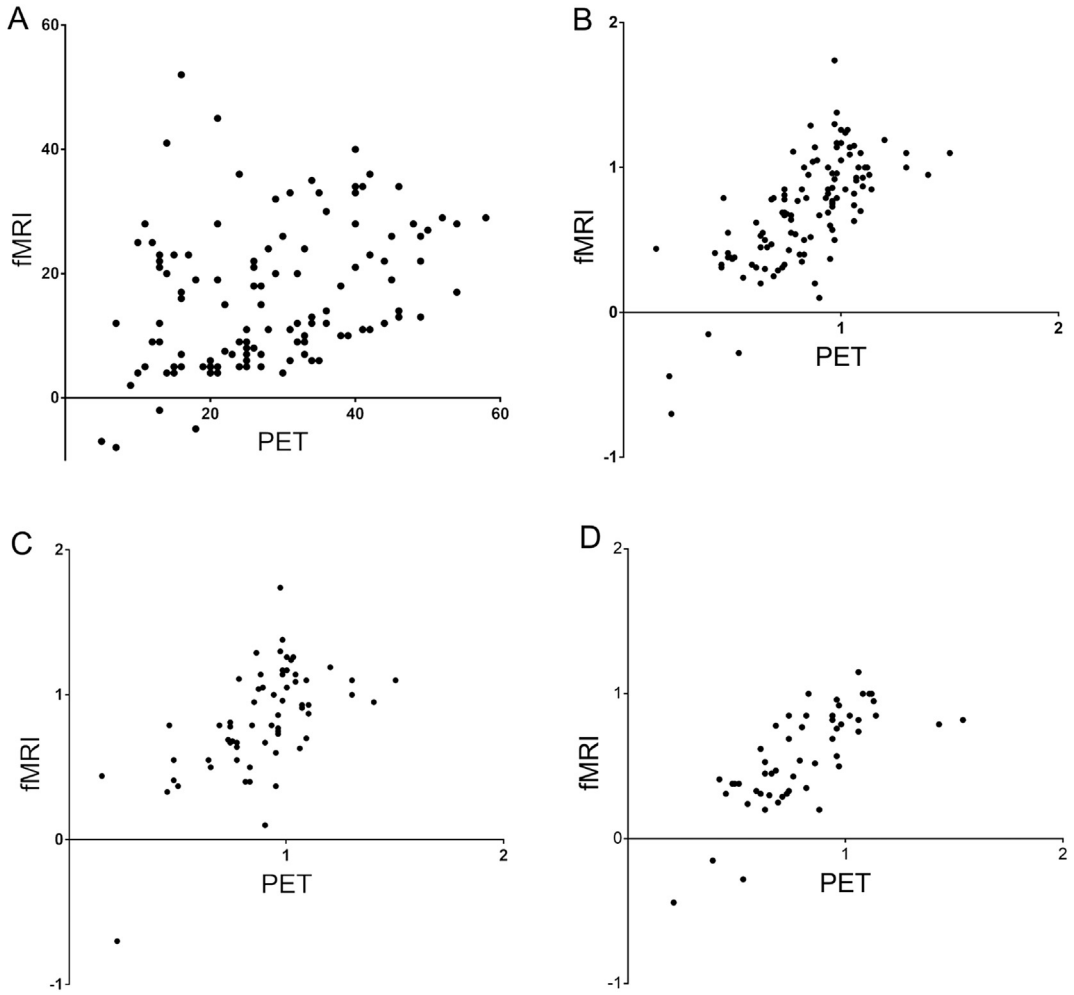

Fig. 2. Plots showing the correlation of all signal changes for PET (x-axis) and fMRI (y-axis). A) shows the correlation of absolute values of signal change showing a weak, but significant correlation ($r = 0.35$, $p = 0.001$). B–D) shows values calculated as the quotient of absolute values in the respective vascular territories and signal of the cerebellum with strong correlation. B) depicts territories of all patients ($r = 0.71$, $p < 0.001$), C) of all patients with preoperative ($r = 0.61$, $p < 0.001$) and D) of all patients with postoperative imaging ($r = 0.76$, $p < 0.001$).

patient should be used with any additional efforts needed. For such efforts, a computer-controlled gas delivery system might be the better choice.

4.2. Risk of wrong estimation of the cerebrovascular reactivity

Visual analysis of color-coded maps of regional cerebrovascular reserve/−reactivity is the most commonly used way to interpret results for the respective territories. In our analysis we did not have a single patient/vascular territory with an entirely discrepant visual estimation of the CVR in comparison to the CPR in PET. If divergent, both modalities did not differ more than one grade of our four-step visual evaluation system.

Further, a special finding of BOLD MRI needs to be mentioned: Negative quotients for vasoreactivity were seen in 4 vascular territories in BOLD MRI. These territories were also severely affected with a significantly decreased perfusion reserve in PET (quotient normalized to the cerebellum below 0.5, which was only be seen in very few territories (see Fig. 2)), yet not negative. Whether such findings in BOLD MRI resemble a vascular stealing phenomenon, or just an artifact by delayed vasodilatation in the acquisition of BOLD MRI, remains uncertain and is discussed controversially in the literature (Mandell et al., 2008; Watchmaker et al., 2019; Fierstra et al., 2010). However, all territories with negative vasoreactivity in BOLD MRI proved to be severely affected in PET CT as well, and would have therefore not resulted in a wrong estimation from a clinical point of view.

On purpose we did not include a cut-off value to indicate a possible surgical revascularization for this analysis, which we also do not use in our current clinical routine with PET. Clinical decision making must always be based on the entire available spectrum of imaging modalities, namely conventional MRI and angiography plus additional quantitative ACZ-challenge cerebrovascular imaging, such as PET, or possibly CO_2-triggered BOLD MRI in the future (see exemplary case Fig. 3).

4.3. Limitations

Main limitation of this study is the retrospective assessment and limited number of patient data for this study. Yet, this is the first series of a patient cohort with angiographically proven MMD and standardized comparison (visual ratings and semi-quantitative analyses) of $H_2{}^{15}O$ PET with ACZ challenge and breath-hold BOLD MRI. The time between both imaging modalities was up to 6 months with no surgical intervention in between. A change in CVR might have occurred in patients within this time, yet this would be a very uncommon rapid disease progression of clinically stable Moyamoya patients. Therefore, we think that this fact may not limit the impact of this study's findings. As discussed above, the breath-hold stimulus might show some inter-individual variation, which however might not be of overriding importance as comparison of changes between pre- and post-stimulus is evaluated in individuals only and not for the entire cohort. It should

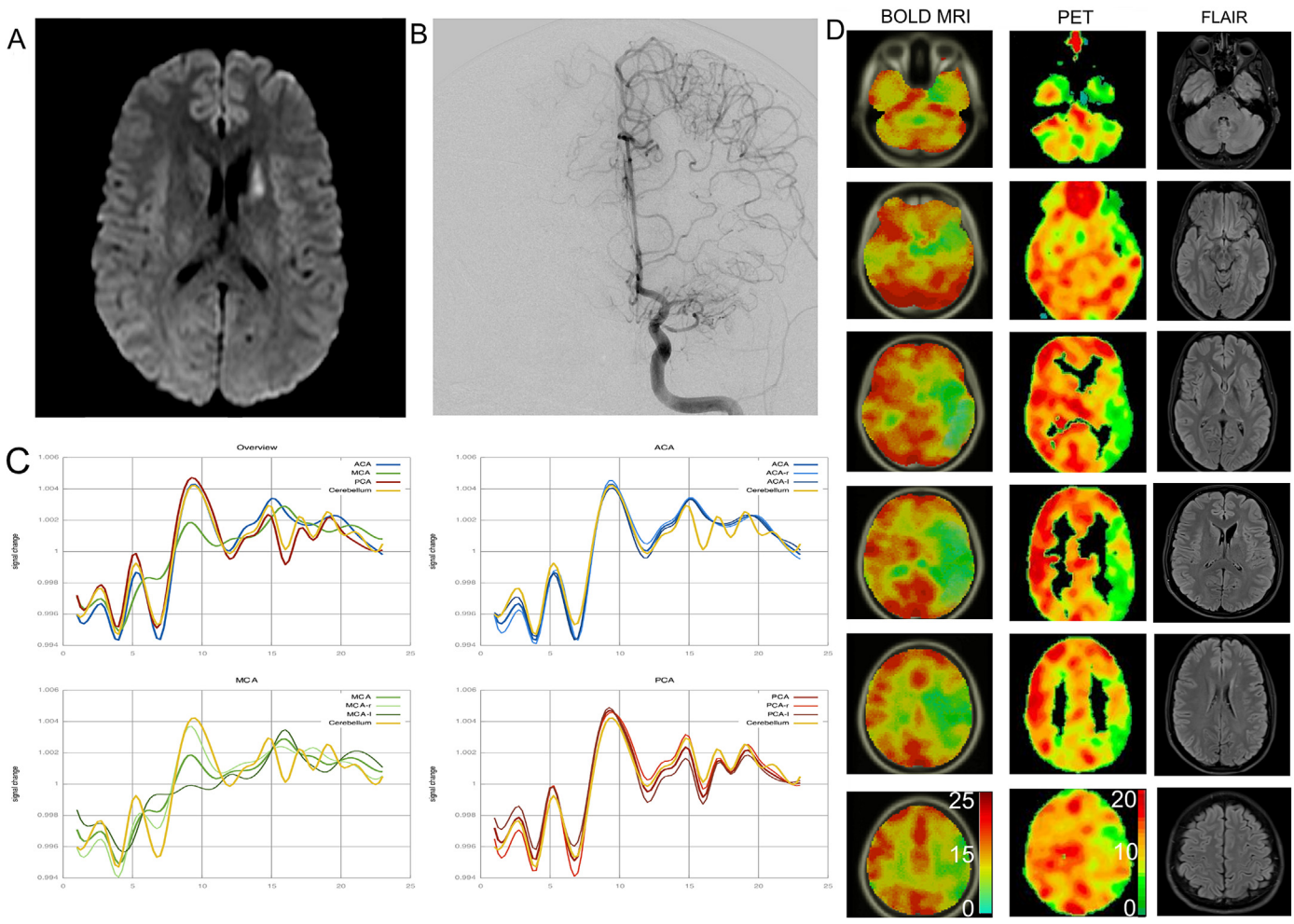

Fig. 3. Exemplary case of a patient with unilateral Moyamoya Angiopathy symptomatic by an infarction in the caudate nucleus (A). Cerebral angiography (B) shows an occlusion of the left MCA with surrounding fine Moyamoya collaterals. C) shows the PSTH of all curves as a mean (top left), as well ACA (blue), MCA (green) and PCA (red) for the respective hemispheres. Significant decrease of vasoreactivity can be seen isolated in the left MCA territory. D) shows the standardized color-coded maps of signal change of breath-hold BOLD MRI (left column) in comparison to $H_2{}^{15}O$ PET/CT (middle column) signal change between baseline and after ACZ administration. Values for the color-scale resemble the integral of the relative signal change of BOLD MRI and absolute signal change (%) of PET. Despite slight differences in the color-scale and slice direction between both modalities, high correlation of both techniques can be seen. Right column shows corresponding FLAIR images. This patient was treated successfully by direct STA-MCA revascularization.

also be addressed that a short breath-hold stimulus of 9 s was used. Therefore, results might be influenced by variable arterial circulation times and collaboration of these patients. However, adequate collaboration of patients is controlled by replicable changes of cerebellar BOLD MRI signal change, making this approach reliable for clinical use, as also shown in other studies (Bright and Murphy, 2013; Dlamini et al., 2018). Further we did not use absolute quantification of CBF by PET, but a simplified approximation of CPR and intra-individual normalized values for comparison with MRI. Future prospective studies, also including absolute quantification of CBF-PET, are needed for proper validation of breath-hold BOLD MRI.

5. Conclusions

CO_2-triggered breath-hold BOLD MRI seems to be a promising tool for the evaluation of the CVR in patients with Moyamoya and correlates well with the results of ACZ-triggered cerebrovascular reserve evaluation on $H_2{}^{15}O$ PET/CT. This technique represents a less expensive and widely available method for the evaluation of hemodynamics in patients with Moyamoya Disease. Further prospective studies are needed to explore its potential as a widely implementable tool for routine clinical imaging.

Sources of funding

None.

Disclosures

None.

References

Acker, G., Lange, C., Schatka, I., Pfeifer, A., Czabanka, M.A., Vajkoczy, P., et al., 2018. Brain perfusion imaging under acetazolamide challenge for detection of impaired cerebrovascular reserve capacity: positive findings with 15o-water pet in patients with negative 99mtc-hmpao spect findings. J. Nucl. Med. 59, 294–298.

Arigoni, M., Kneifel, S., Fandino, J., Khan, N., Burger, C., Buck, A., 2000. Simplified quantitative determination of cerebral perfusion reserve with h 2 15 o pet and acetazolamide. Eur. J. Nucl. Med. Mol. Imaging 27, 1557–1563.

Bright, M.G., Murphy, K., 2013. Reliable quantification of bold fmri cerebrovascular reactivity despite poor breath-hold performance. NeuroImage 83, 559–568.

Diedrichsen, J., 2006. A spatially unbiased atlas template of the human cerebellum. NeuroImage 33, 127–138.

Dlamini, N., Shah-Basak, P., Leung, J., Kirkham, F., Shroff, M., Kassner, A., et al., 2018. Breath-hold blood oxygen level–dependent mri: a tool for the assessment of cerebrovascular reserve in children with moyamoya disease. Am. J. Neuroradiol. 39, 1717–1723.

Donahue, M.J., Dethrage, L.M., Faraco, C.C., Jordan, L.C., Clemmons, P., Singer, R., et al.,

2014. Routine clinical evaluation of cerebrovascular reserve capacity using carbogen in patients with intracranial stenosis. Stroke 45 (8), 2335–2341 STROKEAHA. 114.005975.
Donahue, M.J., Achten, E., Cogswell, P.M., De Leeuw, F.-E., Derdeyn, C.P., Dijkhuizen, R.M., et al., 2018. Consensus statement on current and emerging methods for the diagnosis and evaluation of cerebrovascular disease. J. Cereb. Blood Flow Metab. 38, 1391–1417.
Fierstra, J., Poublanc, J., Han, J.S., Silver, F., Tymianski, M., Crawley, A.P., et al., 2010. Steal physiology is spatially associated with cortical thinning. J. Neurol. Neurosurg. Psychiatry 81, 290–293.
Fierstra, J., Sobczyk, O., Battisti-Charbonney, A., Mandell, D., Poublanc, J., Crawley, A., et al., 2013. Measuring cerebrovascular reactivity: what stimulus to use? J. Physiol. 591, 5809–5821.
Fierstra, J., van Niftrik, C., Warnock, G., Wegener, S., Piccirelli, M., Pangalu, A., et al., 2018. Staging hemodynamic failure with blood oxygen-level–dependent functional magnetic resonance imaging cerebrovascular reactivity. In: A Comparison Versus Gold Standard (^{15}O-)H_2O-Positron Emission Tomography. 49. pp. 621–629.
Guzman, R., Lee, M., Achrol, A., Bell-Stephens, T., Kelly, M., Do, H.M., et al., 2009. Clinical outcome after 450 revascularization procedures for moyamoya disease: Clinical article. J. Neurosurg. 111, 927–935.
Hammers, A., Allom, R., Koepp, M.J., Free, S.L., Myers, R., Lemieux, L., et al., 2003. Three-dimensional maximum probability atlas of the human brain, with particular reference to the temporal lobe. Hum. Brain Mapp. 19, 224–247.
Heyn, C., Poublanc, J., Crawley, A., Mandell, D., Han, J.S., Tymianski, M., et al., 2010. Quantification of cerebrovascular reactivity by blood oxygen level-dependent mr imaging and correlation with conventional angiography in patients with moyamoya disease. AJNR Am. J. Neuroradiol. 31, 862–867.
Kastrup, A., Kruger, G., Neumann-Haefelin, T., Moseley, M.E., 2001. Assessment of cerebrovascular reactivity with functional magnetic resonance imaging: Comparison of co(2) and breath holding. Magn. Reson. Imaging 19, 13–20.
Khan, N., Schuknecht, B., Boltshauser, E., Capone, A., Buck, A., Imhof, H., et al., 2003. Moyamoya disease and moyamoya syndrome: experience in europe; choice of revascularisation procedures. Acta Neurochir. 145, 1061–1071.
Lee, M., Zaharchuk, G., Guzman, R., Achrol, A., Bell-Stephens, T., Steinberg, G.K., 2009. Quantitative hemodynamic studies in moyamoya disease: a review. Neurosurg. Focus. 26, E5.
Liu, P., Welch, B.G., Li, Y., Gu, H., King, D., Yang, Y., et al., 2017. Multiparametric imaging of brain hemodynamics and function using gas-inhalation mri. NeuroImage 146, 715–723.
Mandell, D.M., Han, J.S., Poublanc, J., Crawley, A.P., Stainsby, J.A., Fisher, J.A., et al., 2008. Mapping cerebrovascular reactivity using blood oxygen level-dependent mri in patients with arterial steno-occlusive disease: Comparison with arterial spin labeling mri. Stroke 39, 2021–2028.
Mazerolle, E.L., Ma, Y., Sinclair, D., Pike, G.B., 2018. Impact of abnormal cerebrovascular reactivity on bold fmri: a preliminary investigation of moyamoya disease. Clin. Physiol. Funct. Imaging 38, 87–92.
Mikulis, D.J., Krolczyk, G., Desal, H., Logan, W., Deveber, G., Dirks, P., et al., 2005. Preoperative and postoperative mapping of cerebrovascular reactivity in moyamoya disease by using blood oxygen level-dependent magnetic resonance imaging. J. Neurosurg. 103, 347–355.
Mutsaerts, H.J.M.M., van Dalen, J.W., Heijtel, D.F.R., Groot, P.F.C., Majoie, C.B.L.M., Petersen, E.T., et al., 2015. Cerebral perfusion measurements in elderly with hypertension using arterial spin labeling. PLoS One 10, e0133717.
O'Brien, T.J., O'Connor, M.K., Mullan, B.P., Brinkmann, B.H., Hanson, D., Jack, C.R., et al., 1998. Subtraction ictal spet co-registered to mri in partial epilepsy: Description and technical validation of the method with phantom and patient studies. Nucl. Med. Commun. 19, 31–45.
Pandey, P., Steinberg, G.K., 2011. Neurosurgical advances in the treatment of moyamoya disease. Stroke 42, 3304–3310.
Pellaton, A., Bijlenga, P., Bouchez, L., Cuvinciuc, V., Barnaure, I., Garibotto, V., et al., 2016. Co2bold assessment of moyamoya syndrome: Validation with single photon emission computed tomography and positron emission tomography imaging. World J. Radiol. 8, 887.
Roder, C., Burkle, E., Ebner, F.H., Tatagiba, M., Ernemann, U., Buck, A., et al., 2018. Estimation of severity of moyamoya disease in h2(15)o-pet compared to mri and angiography. World Neurosurg. 117, e75–e81.
Sam, K., Poublanc, J., Sobczyk, O., Han, J.S., Battisti-Charbonney, A., Mandell, D.M., et al., 2015. Assessing the effect of unilateral cerebral revascularisation on the vascular reactivity of the non-intervened hemisphere: a retrospective observational study. BMJ Open 5, e006014.
Scott, R.M., Smith, E.R., 2009. Moyamoya disease and moyamoya syndrome. N. Engl. J. Med. 360, 1226–1237.
Shiino, A., Morita, Y., Tsuji, A., Maeda, K., Ito, R., Furukawa, A., et al., 2003. Estimation of cerebral perfusion reserve by blood oxygenation level—dependent imaging: Comparison with single-photon emission computed tomography. J. Cereb. Blood Flow Metab. 23, 121–135.
Suzuki, J., Takaku, A., 1969. Cerebrovascular "moyamoya" disease. Disease showing abnormal net-like vessels in base of brain. Arch. Neurol. 20, 288–299.
Tatu, L., Moulin, T., Bogousslavsky, J., Duvernoy, H., 1998. Arterial territories of the human brain: Cerebral hemispheres. Neurology 50, 1699–1708.
van Niftrik, C.H.B., Piccirelli, M., Bozinov, O., Pangalu, A., Valavanis, A., Regli, L., et al., 2016. Fine tuning breath-hold-based cerebrovascular reactivity analysis models. Brain Behav. 6, e00426.
Watchmaker, J.M., Frederick, B.D., Fusco, M.R., Davis, L.T., Juttukonda, M.R., Lants, S.K., et al., 2019. Clinical use of cerebrovascular compliance imaging to evaluate revascularization in patients with moyamoya. Neurosurgery 84, 261–271.